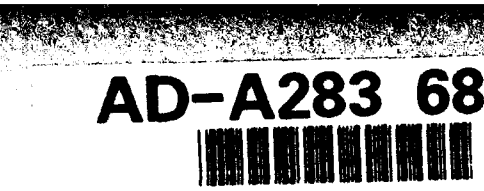

ARMY RESEARCH LABORATORY

Midinfrared Optical Properties of Petroleum Oil Aerosols

by K. P. Gurton
Physical Science Laboratory

C. W. Bruce
Battlefield Environment Directorate

ARL-TR-255

August 1994

NOTICES

Disclaimers

The findings in this report are not to be construed as an official Department of the Army position, unless so designated by other authorized documents.

The citation of trade names and names of manufacturers in this report is not to be construed as official Government indorsement or approval of commercial products or services referenced herein.

Destruction Notice

When this document is no longer needed, destroy it by any method that will prevent disclosure of its contents or reconstruction of the document.

REPORT DOCUMENTATION PAGE

Form Approved
OMB No. 0704-0188

1. AGENCY USE ONLY *(Leave blank)*	2. REPORT DATE	3. REPORT TYPE AND DATES COVERED
	August 1994	Final

4. TITLE AND SUBTITLE

Midinfrared Optical Properties of Petroleum Oil Aerosols

5. FUNDING NUMBERS

6. AUTHOR(S)

K. P. Gurton and C. W. Bruce

7. PERFORMING ORGANIZATION NAME(S) AND ADDRESS(ES)

Physical Science Laboratory
New Mexico State University
Las Cruces, NM 88003

8. PERFORMING ORGANIZATION REPORT NUMBER

9. SPONSORING/MONITORING AGENCY NAME(S) AND ADDRESS(ES)

U.S. Army Research Laboratory
Battlefield Environment Directorate
ATTN: AMSRL-BE-E
White Sands Missile Range, NM 88002-5501

10. SPONSORING/MONITORING AGENCY REPORT NUMBER

ARL-TR-255

11. SUPPLEMENTARY NOTES

12a. DISTRIBUTION/AVAILABILITY STATEMENT

Approved for public release; distribution is unlimited.

12b. DISTRIBUTION CODE

A

13. ABSTRACT *(Maximum 200 words)*

The mass normalized absorption and extinction coefficients were measured for fog oil aerosol at 3.4 μm with a combined photoacoustic and transmissometer system. An extinction spectral profile was determined over a range of infrared (IR) wavelengths from 2.7 to 4.0 μm by an IR scanning transmissometer. The extinction spectrum was mass normalized by referencing it to the photoacoustic portion of the experiment. A corresponding Mie calculation was conducted and compared with the above measurements. Agreement is good for the most recent optical coefficients. An extrapolation of this data to other similar petroleum products such as kerosene or diesel fuel that exhibit similar bulk absorption characteristics were briefly examined.

14. SUBJECT TERMS

midinfrared, aerosol, petroleum, optical, absorption

15. NUMBER OF PAGES
35

16. PRICE CODE

17. SECURITY CLASSIFICATION OF REPORT	18. SECURITY CLASSIFICATION OF THIS PAGE	19. SECURITY CLASSIFICATION OF ABSTRACT	20. LIMITATION OF ABSTRACT
Unclassified	Unclassified	Unclassified	SAR

Acknowledgment

We thank Dr. Gary Eiceman and Mr. Monte Mauldin of the New Mexico State U rsity Chemistry Department for their generous support on the researc ported in this report.

Contents

Figures

Tables

1. Introduction

A petroleum product called fog oil is the primary substance examined. Fog oil is best characterized as a light oil similar to that used to lubricate small machinery. For many years, fog oil has been atomized to produce a fog-like aerosol, most commonly seen in skywriting but also used for many years as an Army obscurant, smoke.

The purpose of this study was to determine absorption and scattering of electromagnetic radiation by this type of hydrocarbon aerosol in an atmospheric transmission window at wavelengths between 3 and 4 μm. Although interest is shown in describing interaction of fog oil aerosol with high-energy laser beams, the optical coefficients are available only in unpublished reports and the values at the wavelengths of interest immensely vary. In this report, the values of n and k for the midinfrared (IR) region are shown to be in reasonable agreement with those of the most recent unpublished report.

The measurements of optical properties are made on fog oil aerosols dispersed and continuously mixed in controlled environmental chambers. Aerosol mass densities and size distributions are determined by using dosimetry and commercially available techniques. Settling characteristics of the well-mixed chamber aerosols yield supportive information regarding the particle size distributions. Mie-theory calculations for the measured size distributions are based on values of the complex refractive indices measured by Weng. [1] The study extends to optical properties for other similar petroleum products.

2. Approach

The approach consisted of two stages:

1. A combination photoacoustical and extinction measurement was performed at the single wavelength of 3.39 μm. Fog oil was nebulized in a controlled environment (chamber) where the absorption and extinction of the aerosol could be determined in situ. Aerosol density and size distribution were concurrently measured. From the optical and dosimetry measurements, the mass normalized absorption and total scattering coefficients were calculated.

2. A relative extinction profile was measured from 2.5 to approximately 12 μm by an IR scanning transmissometer (IRST). The aerosol density and size distribution were determined.

The Mie calculations of the extinction efficiencies at 3.39 μm were based on the previously measured aerosol size distributions and the referenced complex indices. Agreement with the photoacoustic portion of the experiment was good and justified the method of normalizing the relative extinction profile. The result is a continuous, absolute, extinction profile of the aerosol over the region of interest.

A series of Mie calculations spanning the larger range of 2.5 to 12 μm, using the measured size distribution and referenced indices of fog oil, provide comparison with the IRST results.

3. Environmental Chamber for Measurements at 3.4 μm

Fog oil was atomized in a small volume (0.07 m^3) chamber by a De Vilbis pharmaceutical nebulizer. A small fan established and maintained a nearly uniform distribution of particles throughout the chamber. The stirring ensured maintenance of the spatial distribution but was not vigorous enough to significantly alter the size distribution. The photoacoustic system continuously sampled from this plenum.

4. Dosimetry and Size Characterization

Dosimetric measurements were made throughout each experiment to record the aerosol density as a function of time. A Gelman filter holder and filter were inserted into a port projecting into the chamber. Gelman type AE fiberglass filters with a 0.2-μm pore size were used. The volume flow rate (approximately 3 L/min) and the sample time were recorded. The flow rate and sample times were chosen to minimize disturbances and allow collection of a measurable mass amount. The filters were weighed on a Mettler precision balance. Typical mass samples were several milligrams with repeatability of 0.2 mg.

The size distribution for the chamber was characterized in a separate set of measurements. Two types of particle spectrometers were used to characterize the distribution: (1) Particle Measuring System (PMS) model ASASP-X ($0.07 < \text{radius} < 3$ μm, with small orifice) and (2) CSASP-100 ($0.2 < \text{radius} < 16$ μm). A typical size distribution measured in the fixed frequency portion of this experiment is shown in figure 1. The number density distribution with radius is very strongly peaked near a radius of 0.1 μm, and few particles exceed a radius of 5.0 μm.

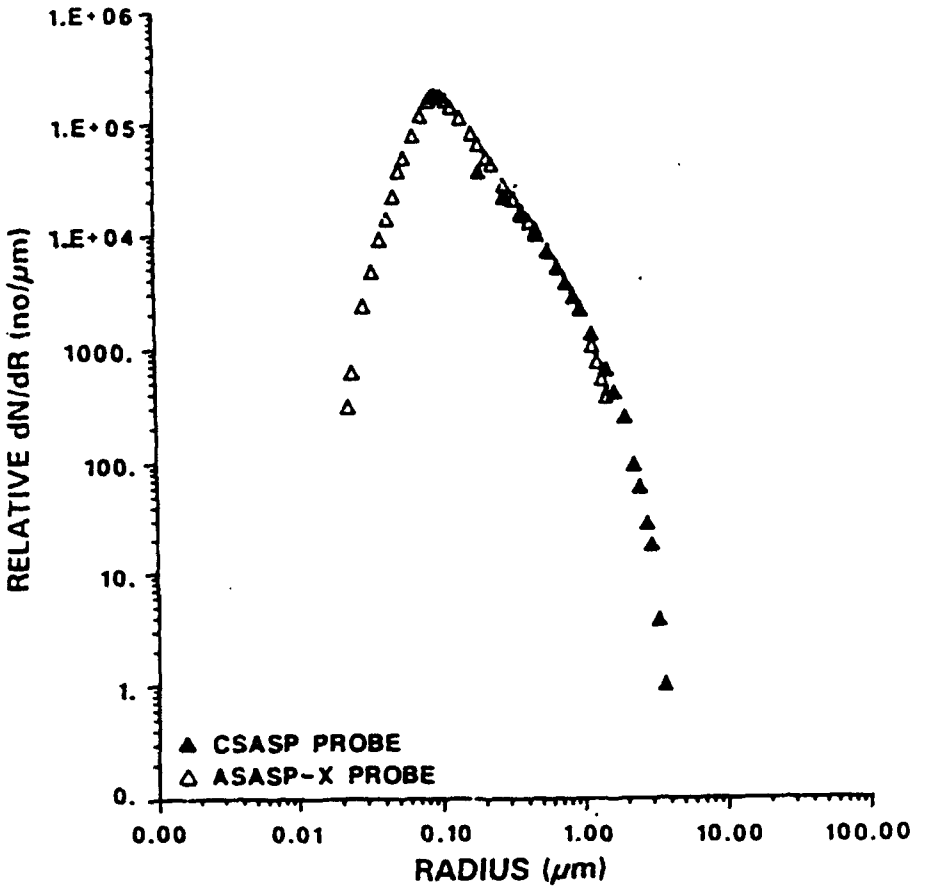

Figure 1. Typical size distribution for aerosol photoacoustic measurements.

5. Photoacoustic Measurements

The photoacoustic and extinction measurements were made with a flow-through photoacoustic unit, described previously by Bruce and Pinnick [2] and Bruce and Richardson, [3] containing a 3.39 μm HeNe laser source, beam positioning optics and a modulator, a cylindrical acoustical cavity with an isolating array of acoustic filters, and a detector.

The laser beam is directed down the axial center of the cavity by two positioning mirrors (figure 2). The laser beam is modulated by a mechanical tuning fork chopper at the fundamental longitudinal resonant frequency of the acoustic cavity. The signal from the microphone embedded centrally in the acoustic cavity wall is amplified with phase-sensitive circuitry. Kreutzer [4] and Trusty [5] show that this signal is linearly proportional to the amount of energy absorbed by the aerosol. The constant proportionality is repeatedly determined by a calibration gas (isopropyl alcohol for 3.4 μm), for which the only significant attenuation is due to absorption.

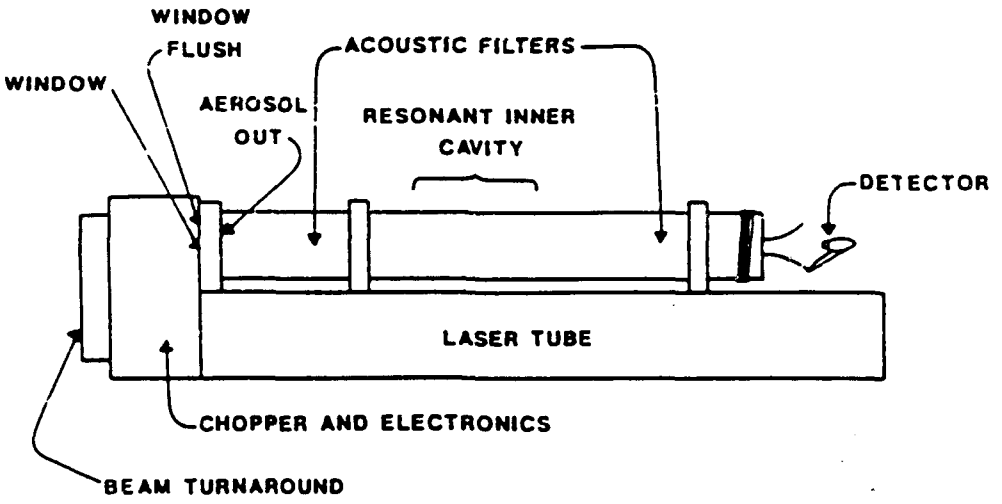

Figure 2. Gas and aerosol spectrophone/transmissometer for 0.63, 1.1, or 3.4 μm.

The beam intensity is monitored by a detector at the opposite end of the cavity. The attenuation by the aerosol is used to calculate the extinction coefficient according to Beer's law, with a forward scattering correction quantified by Deepak and Box. [6]

Aerosol flow through the photoacoustical cavity is regulated and varies from 1 to 3 m/s. During measurement, a valve system alternately selected fresh air and aerosol flow through the spectrophone. This was systematically performed to monitor the unattenuated laser power and establish an intensity baseline. After a uniform flow was achieved, the laser power and spectrophone signal were recorded as a function of time.

From the photoacoustic portion of the experiment the absorption and extinction coefficients as a function of time (figure 3) were measured. The shaded regions represent the dosimetric sampling time intervals. The log averages were taken within the intervals to determine an associated absorption and extinction coefficient (via the absorption calibration constant). An aerosol density was computed for each interval on the basis of the mass samples obtained. Mass normalized efficiencies were calculated from the absorption and extinction coefficients and the aerosol densities at specific times. The forward scattering correction for the measurement geometry and aerosol size distribution of figure 1 is not significant.

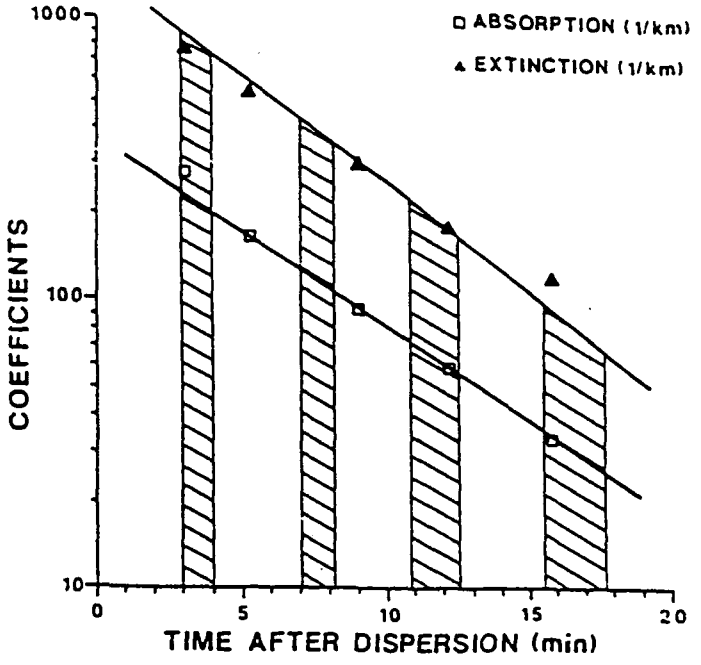

Figure 3. Time evolution of extinction and absorption coefficients.

The average measured and calculated efficiencies at 3.39 μm are shown in table 1. The calculated values are obtained using equation (1) and the measured density distribution.

$$\epsilon = E/_p = \frac{\int \left[\frac{dN}{dr}\right]_i Q_i \pi r^2 \, dr}{\int \left[\frac{dN}{dr}\right]_i \frac{4}{3}\pi r^3 P_B \, dr}, \qquad (1)$$

where

E = extinction coefficient

p = aerosol density

$\left(\frac{dN}{dr}\right)_i$ = number of particles per radius increment

Q_i = Mie coefficient

P_B = bulk density of the aerosol particle

Table 1. Fog oil attenuation efficiencies at 3.39 μm for the size distribution in figure 1

	Measured	Calculated
Absorption	0.483 ±0.03	0.401 ±0.06 (m^2/g)
Total Scattering	0.887 ±0.05	0.809 ±0.12 (m^2/g)

The uncertainties given in table 1 are the one-sigma variations. The uncertainties quoted for the calculated values are solely derived from variations in the size distribution. The measured absorption coefficient is 17 percent higher than calculated, and the total scattering coefficient is 9 percent higher than calculated. Both are within the respective propagated uncertainties, but it is likely (and is illustrated later in this report) that a significant portion of the error results from an uncertainty in the imaginary component of the index of refraction at 3.39 μm.

6. Spectrally Continuous Measurements

Spectrally continuous measurements were conducted in a larger (cubic meter) chamber with two large fans (operating at controlled, reduced rates of rotation) producing an aerosol circulation pattern. Two axial tubes, opposite each other across the center of the chamber, acted as the transmission windows. Fog oil was nebulized in the same manner as the photoacoustic measurements in an effort to produce a size distribution close to that of the 0.07-m^3 chamber. Three pharmaceutical nebulizers were used to atomize the fog oil and produced a particle size distribution similar to the photoacoustic measurement (figure 4). Because the size distributions for both chambers indicate that nearly all the mass was attributable to particles with radii above 0.1 μm (as illustrated in figure 7), the measured mass did not require correction for filter pore size..

A 1000-K glow bar was used as an IR source. Radiation was collimated and focused through the chamber and onto the IRST.

The IRST utilizes a continuously variable circular filter whose resolution depends on the wavelength and the filter quadrant. The wavelength resolution, generally adequate for aerosol spectra, was just barely adequate for this study at 1.3 percent of the 3.39-μm wavelength.

The filtered IR radiation was detected by a Mercury-Cadmium-Telluride detector. The signal was amplified (1000X) and processed by an 8085 microprocessor, and noise reduction schemes such as boxcar integration were applied.

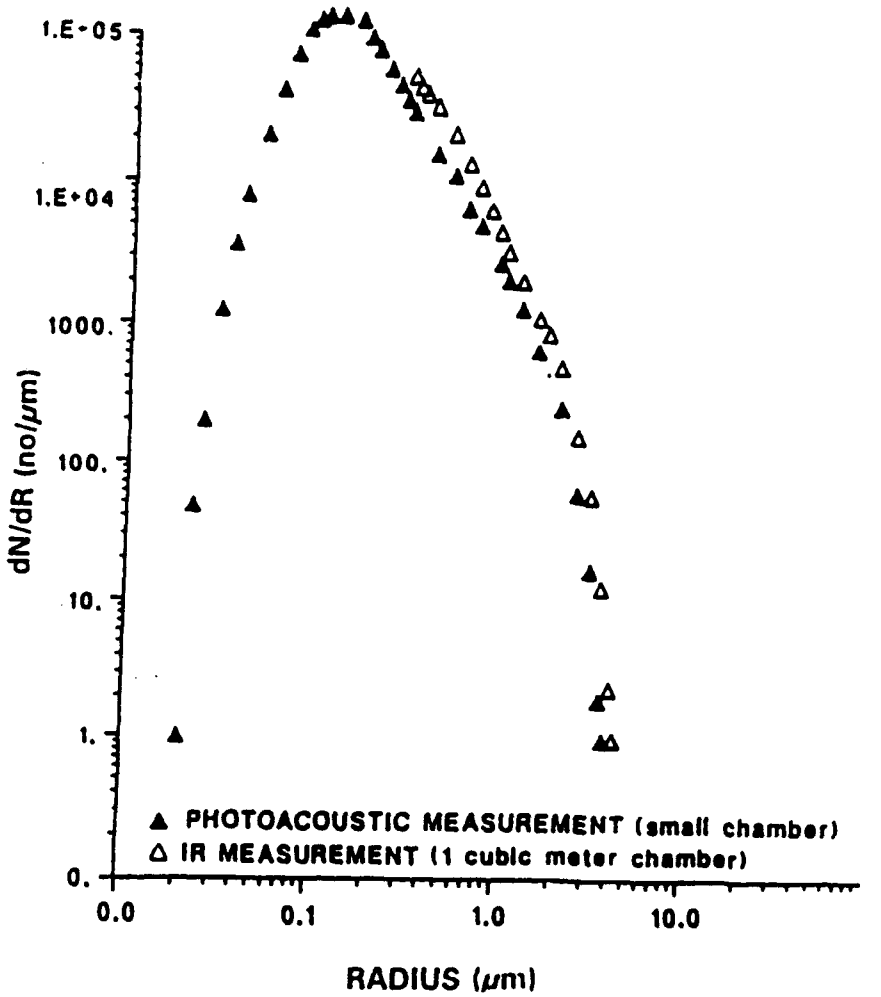

Figure 4. Fog oil particle size distributions for the two chambers.

A relative extinction curve was computed from 2.5 to 4.0 μm using data measured by the IRST. The curve was normalized to the measured absolute extinction efficiency at 3.39 μm.

Figure 5 shows a comparison of the calculated and measured (mass normalized) extinction coefficients for the large chamber.

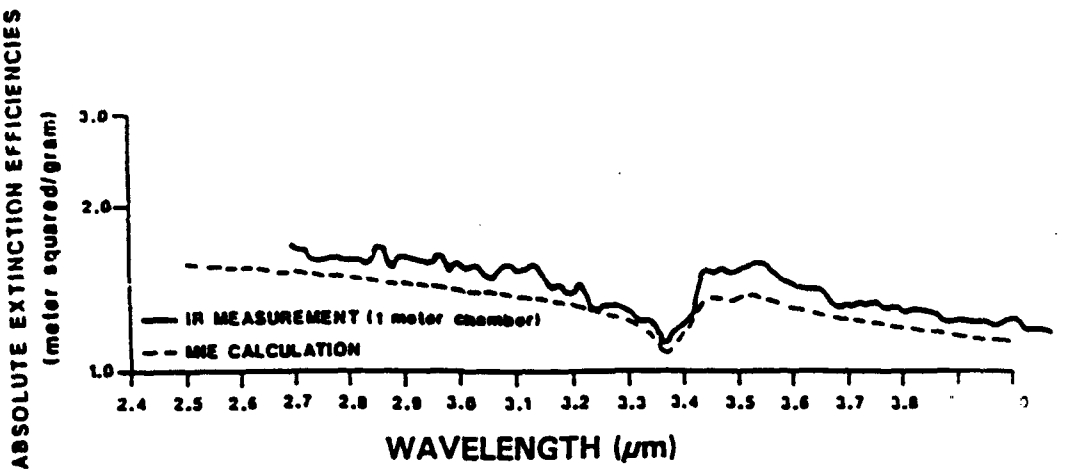

Figure 5. Comparison of calculated (Mie theory) and experimental results.

The line laser absorption measurement falls within the strong adsorption band indicated in figure 5. Structurally, this band results primarily from symmetric and asymmetric stretch bands of CH_3 and CH_2. Spectra presented in Szymanski [7] show that the spectra of fog oil are characteristic of many hydrocarbons and other substances. The net form is presumed to be a superposition of the contributions caused by the liquids of the constituent molecules weighted by their relative occurrence in the presence of the net liquid. Quantitatively, the problem is even more complex than a superposition of the constituents.

It is presumed that discrepancies between the calculated and measured curves arose from uncertainties in the measured size distribution, noise in the spectral measurements, uncertainties in the index measurements, and chemical differences between materials affecting the indices. Fog oil is a term that describes a range of specifications for liquid hydrocarbons identified in a report by Katz et al.; [8] therefore, actual indices may vary.

The previously discussed Mie calculations were expanded to include the absorption efficiencies and were extended out to 12 μm in the plots in figure 6. The plots show that, for the aerosol size distribution produced (probably typical for fog oil), absorption is a minor contribution to the

extinction in the IR. The absorption resonance in the vicinity of 3.4 μm for which the absorption is approximately one-third of the total extinction provides the largest contribution.

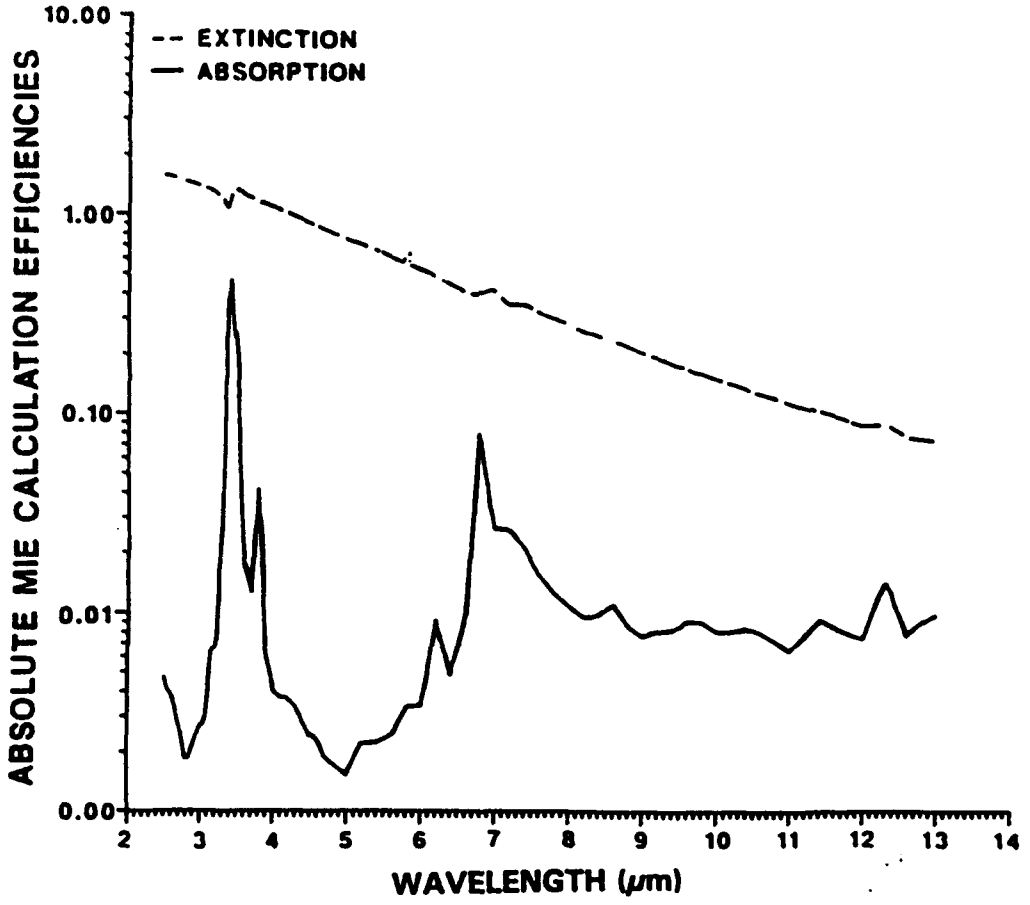

Figure 6. Calculated extinction and absorption spectra of fog oil.

7. Effective Radius of Fog Oil Particles

A rather useful and independent calculation was made to corroborate the experimental results. The calculation involves a method of determining the radii of particles most representative relative to the extinction cross section. The approach is based on an analysis described by Bruce et al. [9] of the settling properties by the time dependent decay of the extinction coefficient. The method considers the rate at which particles of a given size settle out of a well-mixed medium, which can be related to the aerosol aerodynamic cross section. The result yields the radius with the largest contribution to the associated cross section (and through the form of time dependence can give a measure of the size distribution breadth). Settling should not be confused with diffusion, a much slower process for this size distribution. The effective radius was determined using equation (2).

$$\tilde{r} = \sqrt{C} \; x \; S \qquad (2)$$

where

$$C = \frac{9}{2} \frac{(h \; x \; V)}{(\rho_B \; x \; g)}$$

S = slope of the optical coefficient versus time
h = settling height of the chamber
V = viscosity of air
g = acceleration due to gravity.

This calculation of the most representative radius was made for the photoacoustic and the IRST measurements (because the size distributions were slightly different) and the $\tilde{r}$ values for the extinction cross sections were found to be 1.58 $\pm$0.2 μm (photoacoustic, 0.07-m^3 chamber) and 2.10 $\pm$0.2 μm (IRST, 1.0-m^3 chamber).

The $\tilde{r}$ values were compared with the calculated cross sections for each case. The calculated radii correspond very well to the respective curve maxima and further support the integration of the two experiments (figure 7).

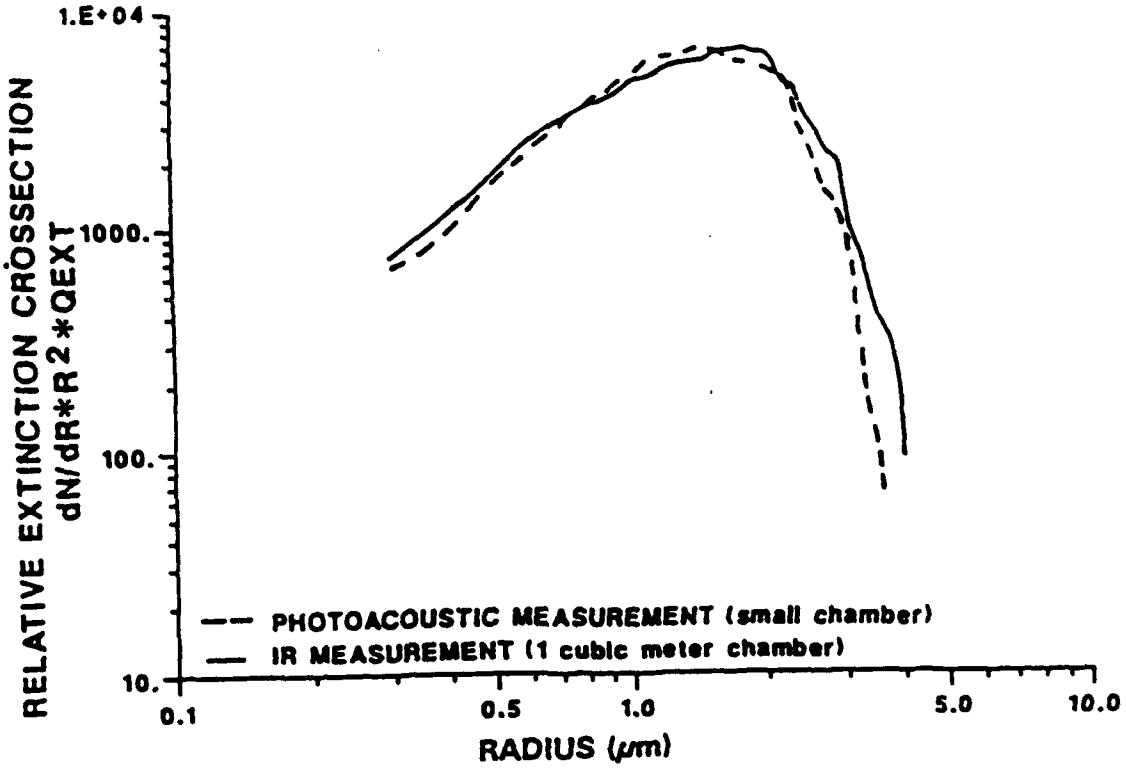

Figure 7. Relative extinction cross section as a function of radius for fog oil aerosol.

8. Inversion of the Mie Process to Determine Complex Index at 3.39 μm

Although the intent was to compare measured values of absorption and total scattering with calculated values from the size distribution and the previously measured complex index, it would perhaps make more sense to reverse the process and accurately determine the values of n and k by an iterative approach using the Mie theory. The inverse approach has been used for several aerosols at various wavelengths and found it to stabilize for the real and imaginary components when a substance exhibits significant absorption and scattering.

Figure 8 illustrates the character of the inversion process for fog oil at 3.39 μm using $\bar{r}$ as the effective particle radius. Selection of a unique pair of values is apparent for the range of indices. The components determined are compared with the previously measured values in table 2. Use of the complete size distribution provides a more accurate determination, but the example in table 2 illustrates the uniqueness of the result.

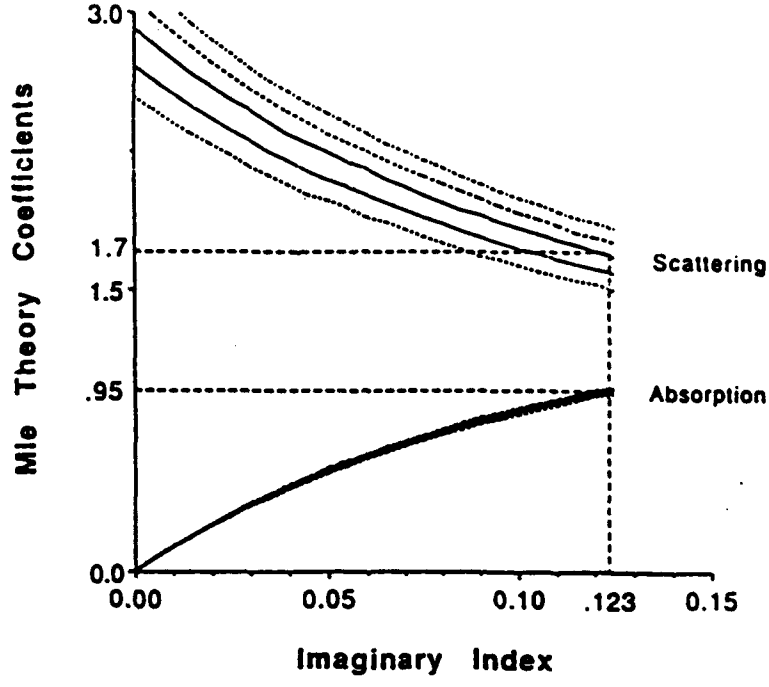

Figure 8. Determination of complex index using Mie theory, effective radius, measured absorption, and total scattering coeffients for fog oil. Mie theory coefficients form an increasing progression as real index increases (for the family of curves) in increments of 0.15.

Table 2. Complex index using the absorption and scattering efficiencies, effective radius, and Mie theory as compared with those of Weng. [1]

	N	K
Calculated	1.425	0.125
Weng [1]	1.450	0.091

9. Chemical and Optical Analysis of Similar Substances

Fog oil and several similar petroleum products were analyzed and an attempt was made to relate fog oil optical properties to the optical properties of other liquids possessing similar hydrocarbon structures.

A Fourier transform IR spectrometer determined the bulk absorption profiles of liquid fog oil, common diesel fuel, and kerosene. The three substances exhibited nearly identical absorption structure within the IR (figure 9a).

The chemical analysis of generic petroleum products is complex. Even relatively simple oils may be composed of many species. In the present investigation, it was sufficient for comparison to characterize each substance by its overall mass profile. Gas chromatography with mass spectroscopy was employed for this procedure. Both the diesel fuel and kerosene had average mass peaks between the C_{12} and C_{14} hydrocarbons, and the less volatile fog oil processed a heavier average mass peak that ranged from C_{22} to C_{24} (figure 9b).

An excellent, thorough chemical characterization was conducted on several different varieties of fog oil by Katz et al. [8] A brief summary of their results follows:

> The results show that fog oil consists of nearly pure hydrocarbons, with the predominant structures being mixtures of aliphatic and aromatic components in almost equal amounts. Also detected were small amounts of alcohols, organic acids, and esters with very small traces of organic nitrogen derivatives. The aliphatic hydrocarbons were in the C_{12} to C_{22} range and the aromatics consisted of 1- through 4-member rings, also within the same range. The results also show that all fog oils contained traces of copper and zinc, with copper near 40 ppb and zinc varying between 20 and 100 ppb. Densities ranged between 0.89 and 0.93 g/ml.
>
> A distinctive color change from clear, light yellow to dark brown over a 24-month period was noted.

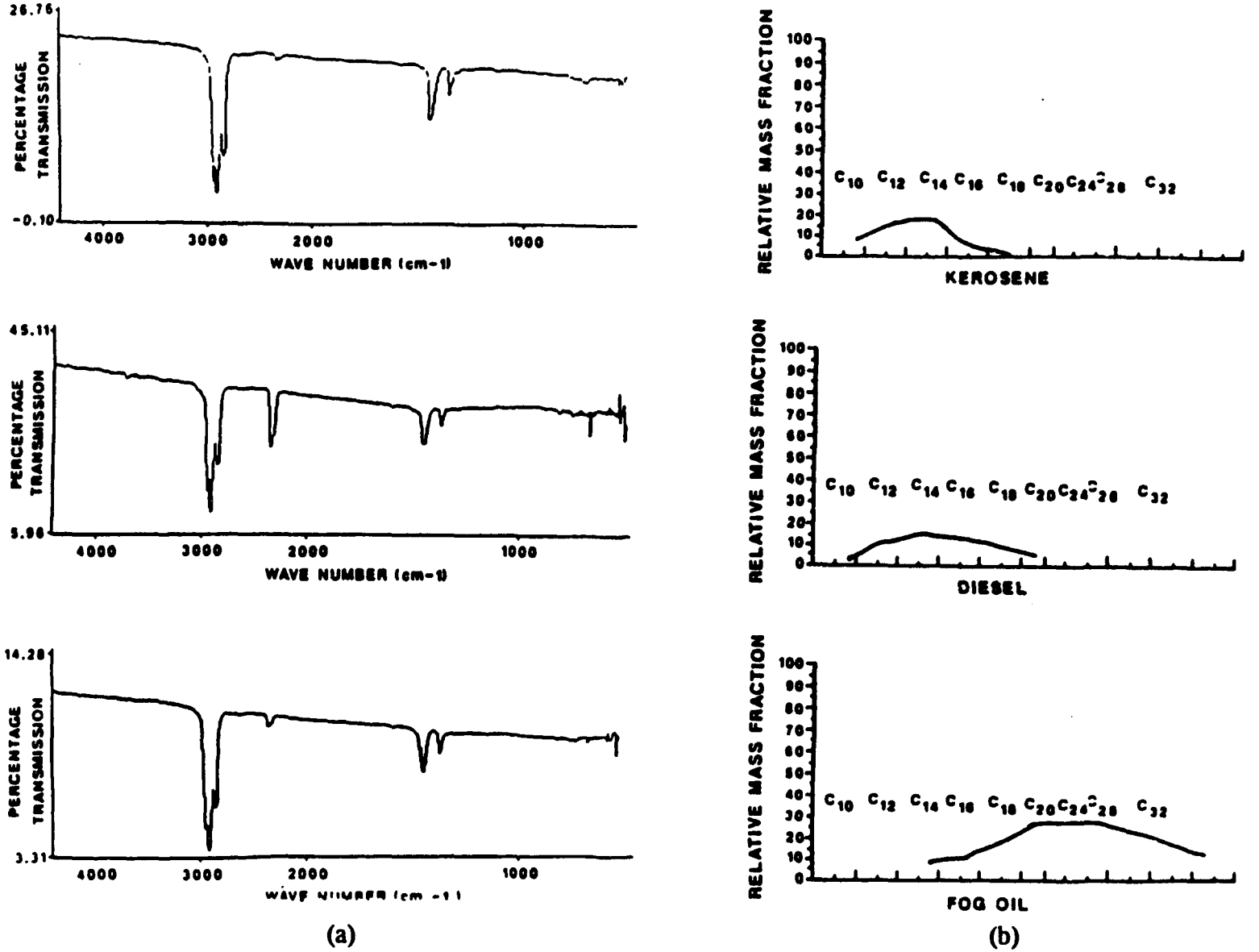

Figure 9. Transmissivity (a) and mass spectra (b) of liquid fog oil, kerosene, and diesel fuel.

10. Comments on the Size Distribution

Measurements were carefully taken to to ensure that, while the medium was well mixed, the size distribution was minimally perturbed in the sampling process.

The instrumental response function of the PMS light scattering counters to the radii of the spherical particles is multivalued in the resonance region; therfore, several different sized particles can yield the same response. According to Pinnick and Auvermann, [10] the multivalued response can create an artificial ripple structure in the size distribution unless particles are categorized in radius ranges designed to avoid causing an artificial ripple structure. The reduction in resolution resulting from the adjustment of radius size increments was not severe for the measured distributions of fog oil.

11. Summary

The absorption and total scattering efficiencies for fog oil aerosol were determined and compared with calculated values for given size distributions. After various parametric studies and analyses, it is considered that most of the uncertainty resides in the size distributions and the indices (the calculated values).

The optical measurements were extended to a continuous wavelength span in the vicinity of 3.39 μm by measuring extinction spectra. Absorption spectra were not measured because available continuous sources do not have sufficient power to drive the photoacoustical measurement. Normalization of the spectrum using the laser result gains credibility because the calculated values are in reasonable agreement with the form of the extinction spectrum and with the absorption and extinction values at the laser line wavelength.

Indicating similarity of optical properties for related liquid hydrocarbons was of interest and was investigated here only for the bulk materials, but the absorption spectra near 3.39 μm were found to be similar for the three substances (liquid fog oil, common diesel fuel, and kerosene).

The measured size distribution was, to a degree, substantiated by agreement with the independent settling theory calculations. The calculation of the effective radius for an optical coefficient agreed well with the peak radius for each distribution and indicated the narrow breadth of the distribution through the small curvature of the semilog plot showing decay of the optical coefficient with time.

The effective radius and the coefficients provided a basis for an independent and accurate determination of the complex index at the line laser wavelength.

References

1. Weng, S., *Complex Refractive Indices of Selected Liquids*, Master's Thesis, University of Missouri-Kansas City, pp 139-140, 1987.

2. Bruce, C. W. and R. G. Pinnick, *Appl Opt*, 16:1762-1764, 1977.

3. Bruce, C. W. and N. M. Richardson, *Appl Opt*, 22:1051-1055, 1983.

4. Kreutzer, L. B., *J. Appl. Phys.*, 42:2934-2943, 1971.

5. Trusty, G. L., *Absorption Measurements of the 10 μm Region Using a CO_2 Laser and a Spectrophone*. Ph.D. dissertation, University of Ohio, 1973.

6. Deepak, A. and M. A. Box, *Appl Opt*, 17:2900-2909, 1978.

7. Szymanski, H. A., *I.R. Theory and Practice of Infrared Spectroscopy*, Consultants Bureau Enterprises, Inc., New York, NY, 1964.

8. Katz, S., A. Snelson, and R. Butler, *Physical and Chemical Characterization of Military Smokes* (part 2), Report No. A093205, U.S. Army Medical Research and Development Command, Fort Detrick, Frederick, MD, 1980.

9. Bruce, C. W., D. Kalinowski, and D. R. Ashmore, *Aerosol Science and Technology*, 12:1031-1035, 1990.

10. Pinnick, R. G. and H. J. Auvermann, *J. Aerosol Sci.*, 10:55-74, 1979.

Acronyms and Abbreviations

IR	infrared
IRST	infrared scanning transmissometer
PMS	Particle Measuring System

DISTRIBUTION

	Copies
Commandant U.S. Army Chemical School ATTN: ATZN-CM-CC (Mr. Barnes) Fort McClellan, AL 36205-5020	1
NASA Marshal Space Flight Center Deputy Director Space Science Laboratory Atmospheric Sciences Division ATTN: E501 (Dr. Fichtl) Huntsville, AL 35802	1
NASA/Marshall Space Flight Center Atmospheric Sciences Division ATTN: Code ED-41 Huntsville, AL 35812	1
Deputy Commander U.S. Army Strategic Defense Command ATTN: CSSD-SL-L (Dr. Lilly) P.O. Box 1500 Huntsville, AL 35807-3801	1
Deputy Commander U.S. Army Missile Command ATTN: AMSMI-RD-AC-AD (Dr. Peterson) Redstone Arsenal, AL 35898-5242	1
Commander U.S. Army Missile Command ATTN: AMSMI-RD-DE-SE (Mr. Lill, Jr.) Redstone Arsenal, AL 35898-5245	1
Commander U.S. Army Missile Command ATTN: AMSMI-RD-AS-SS (Mr. Anderson) Redstone Arsenal, AL 35898-5253	1
Commander U.S. Army Missile Command ATTN: AMSMI-RD-AS-SS (Mr. B. Williams) Redstone Arsenal, AL 35898-5253	1
Commander U.S. Army Missile Command Redstone Scientific Information Center ATTN: AMSMI-RD-CS-R/Documents Redstone Arsenal, AL 35898-5241	1

Commander
U.S. Army Aviation Center
ATTN: ATZQ-D-MA (Mr. Heath) 1
Fort Rucker, AL 36362

Commander
U.S. Army Intelligence Center
and Fort Huachuca
ATTN: ATSI-CDC-C (Mr. Colanto) 1
Fort Huachuca, AZ 85613-7000

Northrup Corporation
Electronics Systems Division
ATTN: Dr. Tooley 1
2301 West 120th Street, Box 5032
Hawthorne, CA 90251-5032

Commander
Pacific Missile Test Center
Geophysics Division
ATTN: Code 3250 (Mr. Battalino) 1
Point Mugu, CA 93042-5000

Commander
Code 3331
Naval Weapons Center
ATTN: Dr. Shlanta 1
China Lake, CA 93555

Lockheed Missiles & Space Co., Inc.
Kenneth R. Hardy
ORG/91-01 B/255 1
3251 Hanover Street
Palo Alto, CA 94304-1191

Commander
Naval Ocean Systems Center
ATTN: Code 54 (Dr. Richter) 1
San Diego, CA 92152-5000

Meteorologist in Charge
Kwajalein Missile Range
P.O. Box 67 1
APO San Francisco, CA 96555

U.S. Department of Commerce Center
Mountain Administration
Support Center, Library, R-51
Technical Reports
325 S. Broadway 1
Boulder, CO 80303

Dr. Hans J. Liebe
NTIA/ITS S 3
325 S. Broadway 1
Boulder, CO 80303

NCAR Library Serials
National Center for Atmos Research
P.O. Box 3000 1
Boulder, CO 80307-3000

Headquarters
Department of the Army
ATTN: DAMI-POI 1
Washington, DC 20310-1067

Mil Asst for Env Sci Ofc of
the Undersecretary of Defense
for Rsch & Engr/R&AT/E&LS
Pentagon - Room 3D129 1
Washington, DC 20301-3080

Headquarters
Department of the Army
DEAN-RMD/Dr. Gomez 1
Washington, DC 20314

Director
Division of Atmospheric Science
National Science Foundation
ATTN: Dr. Bierly 1
1800 G. Street, N.W.
Washington, DC 20550

Commander
Space & Naval Warfare System Command
ATTN: PMW-145-1G 1
Washington, DC 20362-5100

Director
Naval Research Laboratory
ATTN: Code 4110
(Mr. Ruhnke) 1
Washington, DC 20375-5000

Commandant
U.S. Army Infantry
ATTN: ATSH-CD-CS-OR (Dr. E. Dutoit) 1
Fort Benning, GA 30905-5090

USAFETAC/DNE 1
Scott AFB, IL 62225

Air Weather Service
Technical Library - FL4414 1
Scott AFB, IL 62225-5458

USAFETAC/DNE
ATTN: Mr. Glauber 1
Scott AFB, IL 62225-5008

Headquarters
AWS/DOO 1
Scott AFB, IL 62225-5008

Commander
U.S. Army Combined Arms Combat
ATTN: ATZL-CAW 1
Fort Leavenworth, KS 66027-5300

Commander
U.S. Army Space Institute
ATTN: ATZI-SI 1
Fort Leavenworth, KS 66027-5300

Commander
U.S. Army Space Institute
ATTN: ATZL-SI-D 1
Fort Leavenworth, KS 66027-7300

Commander
Phillips Lab
ATTN: PL/LYP (Mr. Chisholm) 1
Hanscom AFB, MA 01731-5000

Director
Atmospheric Sciences Division
Geophysics Directorate
Phillips Lab
ATTN: Dr. McClatchey 1
Hanscom AFB, MA 01731-5000

Raytheon Company
Dr. Sonnenschein
Equipment Division
528 Boston Post Road 1
Sudbury, MA 01776
Mail Stop 1K9

Director
U.S. Army Materiel Systems Analysis Activity
ATTN: AMXSY-CR (Mr. Marchetti) 1
Aberdeen Proving Ground, MD 21005-5071

Director
U.S. Army Materiel Systems Analysis Activity
ATTN: AMXSY-MP (Mr. Cohen) 1
Aberdeen Proving Ground, MD 21005-5071

Director
U.S. Army Materiel Systems Analysis Activity
ATTN: AMXSY-AT (Mr. Campbell) 1
Aberdeen Proving Ground, MD 21005-5071

Director
U.S. Army Materiel Systems
Analysis Activity
ATTN: AMXSY-CS (Mr. Bradley) 1
Aberdeen Proving Ground, MD 21005-5071

Director
ARL Chemical Biology
Nuclear Effects Division
ATTN: AMSRL-SL-CO 1
Aberdeen Proving Ground, MD 21010-5423

Army Research Laboratory
ATTN: AMSRL-D 1
2800 Powder Mill Road
Adelphi, MD 20783-1145

Army Research Laboratory
ATTN: AMSRL-OP-SD-TP 1
Technical Publishing
2800 Powder Mill Road
Adelphi, MD 20783-1145

Army Research Laboratory
ATTN: AMSRL-OP-CI-SD-TL 1
2800 Powder Mill Road
Adelphi, MD 20783-1145

Army Research laboratory
ATTN: AMSRL-SS-SH 1
(Dr. Sztankay)
2800 Powder Mill Road
Adelphi, MD 20783-1145

U.S. Army Space Technology
and Research Office
ATTN: Ms. Brathwaite 1
5321 Riggs Road
Gaithersburg, MD 20882

National Security Agency
ATTN: W21 (Dr. Longbothum) 1
9800 Savage Road
Fort George G. Meade, MD 20755-6000

OIC-NAVSWC
Technical Library (Code E-232) 1
Silver Springs, MD 20903-5000

Commander
U.S. Army Research office
ATTN: DRXRO-GS (Dr. Flood) 1
P.O. Box 12211
Research Triangle Park, NC 27009

Dr. Jerry Davis
North Carolina State University
Department of Marine, Earth, and
Atmospheric Sciences 1
P.O. Box 8208
Raleigh, NC 27650-8208

Commander
U.S. Army CECRL
ATTN: CECRL-RG (Dr. Boyne) 1
Hanover, NH 03755-1290

Commanding Officer
U.S. Army ARDEC
ATTN: SMCAR-IMI-I, Bldg 59 1
Dover, NJ 07806-5000

Commander
U.S. Army Satellite Comm Agency
ATTN: DRCPM-SC-3 1
Fort Monmouth, NJ 07703-5303

Commander
U.S. Army Communications-Electronics
Center for EW/RSTA
ATTN: AMSEL-EW-MD 1
Fort Monmouth, NJ 07703-5303

Commander
U.S. Army Communications-Electronics
Center for EW/RSTA
ATTN: AMSEL-EW-D 1
Fort Monmouth, NJ 07703-5303

Commander
U.S. Army Communications-Electronics
Center for EW/RSTA
ATTN: AMSEL-RD-EW-SP 1
Fort Monmouth, NJ 07703-5206

Commander
Department of the Air Force
OL/A 2d Weather Squadron (MAC) 1
Holloman AFB, NM 88330-5000

PL/WE 1
Kirtland AFB, NM 87118-6008

Director
U.S. Army TRADOC Analysis Center
ATTN: ATRC-WSS-R 1
White Sands Missile Range, NM 88002-5502

Director
U.S. Army White Sands Missile Range
Technical Library Branch
ATTN: STEWS-IM-IT 3
White Sands Missile Range, NM 88002

Army Research Laboratory
ATTN: AMSRL-BE (Mr. Veazy) 1
Battlefield Environment Directorate
White Sands Missile Range, NM 88002-5501

Army Research Laboratory
ATTN: AMSRL-BE-A (Mr. Rubio) 1
Battlefield Environment Directorate
White Sands Missile Range, NM 88002-5501

Army Research Laboratory
ATTN: AMSRL-BE-M (Dr. Niles) 1
Battlefield Environment Directorate
White Sands Missile Range, NM 88002-5501

Army Research Laboratory
ATTN: AMSRL-BE-W (Dr. Seagraves) 1
Battlefield Environment Directorate
White Sands Missile Range, NM 88002-5501

USAF Rome Laboratory Technical
Library, FL2810 1
Corridor W, STE 262, RL/SUL
26 Electronics Parkway, Bldg 106
Griffiss AFB, NY 13441-4514

AFMC/DOW 1
Wright-Patterson AFB, OH 03340-5000

Commandant
U.S. Army Field Artillery School
ATTN: ATSF-TSM-TA (Mr. Taylor) 1
Fort Sill, OK 73503-5600

Commander
U.S. Army Field Artillery School
ATTN: ATSF-F-FD (Mr. Gullion) 1
Fort Sill, OK 73503-5600

Commander
Naval Air Development Center
ATTN: Al Salik (Code 5012) 1
Warminister, PA 18974

Commander
U.S. Army Dugway Proving Ground
ATTN: STEDP-MT-M (Mr. Bowers) 1
Dugway, UT 84022-5000

Commander
U.S. Army Dugway Proving Ground
ATTN: STEDP-MT-DA-L 1
Dugway, UT 84022-5000

Defense Technical Information Center
ATTN: DTIC-OCP 2
Cameron Station
Alexandria, VA 22314-6145

Commander
U.S. Army OEC
ATTN: CSTE-EFS 1
Park Center IV
4501 Ford Ave
Alexandria, VA 22302-1458

Commanding Officer
U.S. Army Foreign Science & Technology Center
ATTN: CM 1
220 7th Street, NE
Charlottesville, VA 22901-5396

Naval Surface Weapons Center
Code G63 1
Dahlgren, VA 22448-5000

Commander and Director
U.S. Army Corps of Engineers
Engineer Topographics Laboratory
ATTN: ETL-GS-LB 1
Fort Belvoir, VA 22060

U.S. Army Topo Engineering Center ATTN: CETEC-ZC Fort Belvoir, VA 22060-5546	1
Commander USATRADOC ATTN: ATCD-FA Fort Monroe, VA 23651-5170	1
TAC/DOWP Langley AFB, VA 23665-5524	1
Commander Logistics Center ATTN: ATCL-CE Fort Lee, VA 23801-6000	1
Science and Technology 101 Research Drive Hampton, VA 23666-1340	1
Commander U.S. Army Nuclear and Chemical Agency ATTN: MONA-ZB, Bldg 2073 Springfield, VA 22150-3198	1
Record Copy	3
Total	89